Sophorolipids-functionalized iron oxide nanoparticles

Niki Baccile, Romain Noiville, Lorenzo Stievano, Inge van Bogaert

▶ **To cite this version:**

Niki Baccile, Romain Noiville, Lorenzo Stievano, Inge van Bogaert. Sophorolipids-functionalized iron oxide nanoparticles. Physical Chemistry Chemical Physics, 2013, 15 (5), pp.1606-1620. 10.1039/C2CP41977G . hal-00770911

HAL Id: hal-00770911
https://hal.science/hal-00770911v1

Submitted on 3 Feb 2017

HAL is a multi-disciplinary open access archive for the deposit and dissemination of scientific research documents, whether they are published or not. The documents may come from teaching and research institutions in France or abroad, or from public or private research centers.

L'archive ouverte pluridisciplinaire **HAL**, est destinée au dépôt et à la diffusion de documents scientifiques de niveau recherche, publiés ou non, émanant des établissements d'enseignement et de recherche français ou étrangers, des laboratoires publics ou privés.

IMPORTANT NOTE : Please be aware that slight modifications occurring after Proof correction may occur between this version of the manuscript and the version on the Publisher's website----------

Sophorolipids-functionalized iron oxide nanoparticles

Niki Baccile,[a,b,c,*] Romain Noiville,[a,b,c] Lorenzo Stievano,[d] Inge Van Bogaert[e]

a - UPMC Univ Paris 06, UMR 7574, Chimie de la Matière Condensée de Paris, F-75005, Paris, France

b - CNRS, UMR 7574, Chimie de la Matière Condensée de Paris, F-75005, Paris, France

c - Collège de France, UMR 7574, Chimie de la Matière Condensée de Paris, F-75005, Paris, France

d - Institut Charles Gerhardt Montpellier - AIME, UMR5253, Université Montpellier II, CC. 1502, Place E. Bataillon, F-34095, Montpellier cedex 5, France

e - InBio, Department of Biochemical and Microbial Technology, Faculty of Bioscience Engineering, Ghent University, Coupure Links 653, 9000, Ghent, Belgium

Abstract

Functional iron oxide nanoparticles (NP) have been synthesized in a one and two-steps method using a natural functional glycolipid belonging to the family of sophorolipids (SL). These compounds, whose open acidic form is highly suitable for nanoparticle stabilization, are readily obtained by a fermentation process of the yeast *Candida bombicola* (polymorph *Starmerella bombicola*) in large amounts. The final carbohydrate coated iron oxide nanoparticles represent interesting potentially biocompatible materials for biomedical applications. According to the synthesis strategy, magnetic properties can eventually be tuned, thus putting in evidence the direct effect of the glycolipid on the final material's structure (maghemite and ferrihydrite have been obtained here). A combination of FT-IR, Dynamic Light Scattering (DLS) and UV-Vis experiments show that SL complex the nanoparticle surface via their accessible COOH group thus forming stable colloids, whose hydrodynamic

diameter mostly varies between 10 nm and 30 nm, both in water and in KCl-containing (0.01 M and 2M) solutions. The materials can stand multiple filtration steps (up to 10) at different extents, where the largest recorded average aggregate size is 100 nm. In general, materials synthesized at T= 80°C display better stability and smaller size distribution than those obtained at room temperature.

Introduction

Multifunctional "smart" nanoparticles for biomedical applications constitute a domain of intense research where multiple materials and properties meet at the same time.[1] In this field, magnetic nanoparticles, and in particular iron oxide-based materials, occupy a special role because of their use in Magnetic Resonance Imaging (MRI) and magnetic hyperthermia applications.[2] Tailoring the surface chemistry of iron oxide nanoparticles allows to enhance and combine different properties, such as colloidal stability in aqueous environment, biocompatibility, low or non-existant toxicity, stealth effects towards physiological barriers (blood, liver, spleen, etc…) and cellular targeting, etc.[2a,c,3] To achieve part, or all, of these properties simultaneously, size control between 10 and 100 nm (to assure for long blood circulation times) and a surface multi-functional approach is generally employed, in addition to a more classical control of crystal structure and homogeneity, shape, etc. Surfactants are generally used to improve colloidal stability in water because many nanoparticle syntheses are performed in organic media. Furthermore, neutral polymers such as polyethylene oxide or dextran are employed as stealth coating agents to pass physiological barriers, while proteins, enzymes, antibodies, or nucleotides are the most common cell targeting agents.[3,4] The success of such a multimolecular approach is demonstrated by the fact that some iron oxide nanoparticle systems have already been approved for clinical trials[2b,3,5] but their intrinsic complexity actually stimulates a research towards simpler nanosystems where the number of multifunctional surface agents is reduced to a minimum, if possible.

Some recent works have shown the possibility to combine some of these properties using carbohydrate to functionalize nanoscale objects,[6] where the functions of selected nanomaterials (carriers, contrast agent, luminescent probe) are combined with sugars. Carbohydrates bring several advantages like water solubility, biocompatibility and, in some cases, specific protein-targeting properties.[7] This new pathway is based on the use of glycoconjugates which have a desired sugar-based moiety covalently connected to an organic spacer. Penades *et al*. have used several techniques to coat gold nanoparticles and surfaces with functionalized glycolipids and to explore the carbohydrate-carbohydrate interactions

tuning the nature of the sugar moiety.[6b] Specific interactions between magnetic nanoparticles and cancer cell lines were investigated by El-Boubbou *et al*.[6a] More complex sugar-functionalized silica-coated nanoparticles have been developed as well, where the silica serves as covalent binding layer through silane-based coupling agents (amide bonding, click-chemistry, etc…) between the nanoparticle and the carbohydrate-containing compound.[8] These works share some features: 1) glycoconjugates are specifically designed *ad-hoc*; 2) the nature of the carbohydrate is tuned according to the desired function (e.g., protein targeting); 3) the synthesis of the glyco-nanoparticles is composed of multiple steps where the glycoconjugate is synthesized first, then the nanoobject is made and finally functionalization is performed to build the glyco-nanomaterial. To this regard, different ways of grafting glycoconjugates have been tested: thiol-chemistry, amide coupling, click-chemistry, etc…

The "glyco" approach shows a number of advantages with respect to the multimolecular pathways discussed in the first paragraph. On one hand, tuning the end-chain functional group (thiol, carboxylic acid, amine, etc…) allows a larger variety of functionalizable surfaces; on the other hand, tuning the nature of the carbohydrate may influence solubility and biocompatibility. Nevertheless, despite these advantages, the synthesis of glycoconjugates is somewhat tedious, time-consuming, expensive and unsustainable. For instance, several functional glycoconjugates of lactose, maltose and glucose reported by Barientos *et al*.[6b] can be obtained in no less than 5 steps, which involve, among others, highly toxic chemical compounds like azobisisobutyronitrile.

In this work we would like to promote the glycoconjugate strategy in combination with iron oxide nanoparticle functionalization by bringing it one step further: instead of using tailored, chemo-derived, glycolipids, we test the open acidic form of sophorolipids (SL), which are biologically-derived glycoconjugates with a well-defined molecular structure given in Scheme 1.

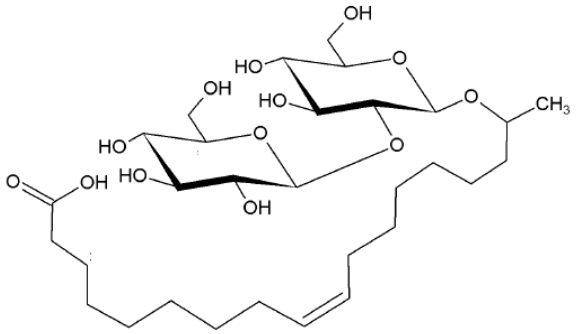

Scheme 1 - Acidic form of sophorolipids (SL) obtained from *Candida bombicola*

These compounds are synthesized by the yeast *Candida bombicola* and have been used so far for detergents[9] and skin care[10] applications. More recent anticancer,[11] antibacterial, self-assembly,[12,13,14] templating and metal-complexing properties[15] have been also put in evidence. SL, in their open acidic form, are composed of a sophorose unit (*i.e.* 2-*O*-β-D-glucopyranosyl-D-glucopyranose; β–Glc-(1-2)-Glc), attached to oleic acid through an ether bond on the C17 carbon atom of the fatty acid chain, thus leaving the COOH group accessible. Hence, acidic SL are water-soluble, non-toxic, biocompatible and the COOH becomes an interesting functional, surface-binding, group. Sophorolipids are produced in large quantities from crops-based resources using a white biotechnology route, constituting a large advantage from an environmental point of view with respect to a chemical engineering approach.

In the field of microbially-derived glycoconjugates, few examples actually exist where specific glycolipids have been used as functional groups for nanoparticles. The main works were carried out by the group of Prasad where cobalt,[15b] silver[15a] and gold[16] nanoparticles were synthesized using the acidic form of sophorolipids. In particular, they have shown that sophorolipids are able to reduce metal salts (Ag, Au) *in-situ*[15a] and to stabilize the corresponding metal nanoparticles in water. Antibacterial and cytotoxic properties of sophorolipids-capped nanoparticles were also studied.

These works have the advantage of showing that sophorolipids can be successfully used as metal nanoparticle stabilizers but many questions are still open: can sophorolipids be employed in metal oxide nanoparticle synthesis? Can they be used in a one-step process? If so, is there any influence on the resulting metal oxide structure? Previous works were always carried out at very dilute sophorolipid and metal concentrations (10^{-3} - 10^{-4} M). Is it possible to work with more concentrated SL and metal salt solutions keeping a good colloidal

dispersion in aqueous solutions? Is the sophorose group readily accessible and can it be exploited further? The full answer to all these questions will undoubtedly open new perspectives for the use of microbial glycoconjugates as nanoparticle functional agents for biomedical applications.

In this work, we show that acidic sophorolipids are suitable compounds to be used as surface complexing agents in the synthesis of iron oxide nanoparticles (NP) in one and two-steps syntheses. In particular, we use more concentrated solutions of metal salts and SL ($5 \cdot 10^{-2}$ M) showing that stable colloidal solutions of iron oxide nanoparticles can easily be synthesized. We show that the choice of the synthesis method has a clear influence on the final metal oxide crystalline structure, on the magnetic properties and particle size distribution. Dynamic Light Scattering (DLS) experiments indicate that sophorolipids-derived nanoparticles exhibit an excellent colloidal stability both in water and in salt-containing aqueous solutions.

Experimental

Synthesis of SL. Sophorolipids were produced by *Candida bombicola* ATCC 22214 using a known procedure.[17] Details on their synthesis can be found in the Supplementary Information material.

Sample preparation. Iron oxide nanoparticles were synthesized using the co-precipitation method following a classical[18] procedure employed to obtain the inverse spinel structure typically observed in magnetite, where $[Fe^{2+}]/[Fe^{3+}]= 0.5$. According to the order of adding the reactants, we have tested two procedures in which the base is added either before or after mixing iron salts with SL. *One-step* (1S): 0.177 g of $FeCl_3 \cdot 6H_2O$ were mixed with 0.108 g of $FeCl_2 \cdot 4H_2O$ in round-bottom flask containing 20 mL of MilliQ water and 0.409 g of the acidic form of sophorolipid. To this solution, about 2.7 mL of a 37 % ammonia solution was added under mechanical stirring. The system was kept under argon to limit oxidation and two temperatures were employed, room temperature (T= RT) and T= 80°C. These samples are referred to as, respectively, 1S-RT and 1S-80C. *Two-steps* (2S): same as above but sophorolipids were added to the mixture only after addition of the ammonia solution and precipitation of the iron oxide nanoparticles. The samples are here referred to as 2S-RT and 2S-80C. In both cases, after one hour, the black precipitate was extracted by centrifugation and washed with water of MilliQ quality. This operation was repeated three times in order to completely eliminate any residual salts.

DLS experiments. Typically, 30 μL of all as-synthesized stock solutions obtained after synthesis were diluted in 1.5 mL of the corresponding medium (pure MilliQ water, water:ethanol=80:20 v:v, KCl in water: 0.01 M, 2 M). The analysis was done on solutions that went through filtering through 0.20 μm nylon membrane. For the experiments shown in Figure 4c-d, 50, 100, 300, 500 mg of a washed and dried maghemite powder, obtained from the two-steps synthesis procedure described above without addition of SL, were mixed with 10 mL of MilliQ water to which 500 mg of acidic sophorolipids were dissolved providing a resulting NP/SL mass ratio of 0.1, 0.3, 0.6, 1.0. In this last set of experiments, all solutions were analyzed at constant shutter opening diameter in the DLS apparatus. For all experiments, number-weighted size distributions are presented in this work and were obtained using the Zetasizer software package in which water was selected as dispersant and where the diffractive index was set to 2.4, which is the typical value for bulk maghemite and magnetite. Each sample was recorded between 3 and 6 times, according to the quality of the data. For multiple filtration experiments, the same filter was employed for each solution in order to minimize the interactions between the nanoparticles and the nylon support.

Other experimental techniques. Transmission Electron Microscopy was performed on a FEI Tecnai 120 Twin microscope operating at 120 kV and equipped with a high resolution Gatan Orius CCD 4k x 4k numeric camera. DigitalMicrograph™ software was used for image acquisition. Dynamic light scattering measurements were run on a Malvern Zetasizer Nano ZS instrument (λ= 633 nm).

UV-Vis adsorption experiments were run on a UVIKON-XL (Secomam) spectrometer using a wavelength scan mode between 300 nm and 800 nm. For the sample preparation of each measurement, refer to the DLS experiment section above. Two steps and one-step samples were systematically analyzed using, respectively, a 1-cm and 0.5-cm path length cuvette. Water absorbance was used as a baseline.

Chemical analysis was obtained by energy dispersive X-ray spectroscopy (EDAX) using an Oxford X-Max (area: 20 mm2) detector installed on a Hitachi S3400N scanning electron microscope. Calibration of the instrument was performed on the Ti Kα at 4.509 keV. Data were obtained and averaged out after acquisition on at least four different sections of the sample distributed throughout the SEM support. Fourier-Transform Infra-Red (FT-IR) spectroscopy has been operated on a Perkin Elmer 400 spectrometer using the universal ATR sampling holder. The powder X-ray diffraction (XRD) study was performed on a Bruker D8 Advance diffractometer using Cu-Kα radiation (λ = 1.5418 Å) at 45 kV and 40 mA, 0.05°

step size and 60 s per step over a 2θ range from 20° to 70°. Thermo Gravimetric Analysis (TGA) was performed on a NETZSCH STA409PC LUXX instrument under air using a 10°C/min heating ramp up to 600°C. The amount of residual matter after treatment at 600°C of the stock solutions has been used to calculate the approximate iron oxide concentration. From TGA one can estimate the area per molecule according to Eq.2 in Supplementary Information.

^{57}Fe Mössbauer spectra were measured with a ^{57}Co:Rh source. During the measurements, both the source and the absorber were kept at ambient temperature (294 K). The spectrometer was operated with a triangular velocity waveform, and a NaI scintillation detector was used for the detection of the gamma rays. The spectra of the measured materials were fitted to appropriate combination of Lorentzian profiles by least-squares methods using the program PC-Mos II.[19]In this way, spectral parameters such as the hyperfine magnetic field (B), quadrupole splitting and shift (Δ and ε, respectively), and isomer shift (δ) were determined. Isomer shifts are given relative to α-Fe metal.

Results and discussion

Materials structure. The co-precipitation method used to synthesize magnetic iron oxide nanoparticles (magnetite structure) is a well-established protocol that we could easily reproduce in the two-steps procedure, where sophorolipids were added only after the ammonia solution and nanoparticle precipitation.[18] The XRD diffraction pattern of the 2S-80C sample (Figure 1) shows the following d-values: 2.967, 2.527, 2.092, 1.714, 1.614, 1.478 Å, corresponding, respectively, to the (220), (311), (400), (422), (511), (440) Bragg diffraction planes of the iron oxide spinel cubic structure (JCPDS file, N° 19-0629) and attributed to maghemite according to Mossbauer arguments (Figure S1 in Supplementary Information). A comparison with the corresponding control, sophorolipid-free, experiment reported in Figure 1 shows that the use of sophorolipid has no influence on the material structure in the 2-step synthesis. The magnetic nature of samples 2S-RT and 2S-80C can be easily evidenced by a simple external magnet, by which the powder grains are promptly attracted both in solution and in their dried form. On the contrary, the product 1S-80C, obtained from the one-step synthesis procedure, has a different XRD pattern, where only two peaks with very broad full-width at half maximum (FWHM) and corresponding to d-values= 2.527 and 1.478 Å are clearly visible. Even if such peaks could be attributed to a classical line broadening effect due to particle size effects and most likely related to the presence of sophorolipids in the reacting medium, the XRD pattern presented here is actually typical of 2-

line ferrihydrite, [$Fe_5HO_8 \cdot (4H_2O)$],[20] as confirmed by ^{57}Fe Mössbauer spectroscopy (Figure S1 and related discussion in Supplementary Information). The corresponding materials synthesized at room temperature exhibit very similar XRD diffraction pattern for both procedures, indicating that temperature has no particular influence on the resulting crystal structure, contrary to the presence of sophorolipids in the reaction mixture. Differently from 2S-RT and 2S-80C, samples 1S-RT and 1S-80C are not attracted by an external magnet, as expected for 2-line ferrihydrite.

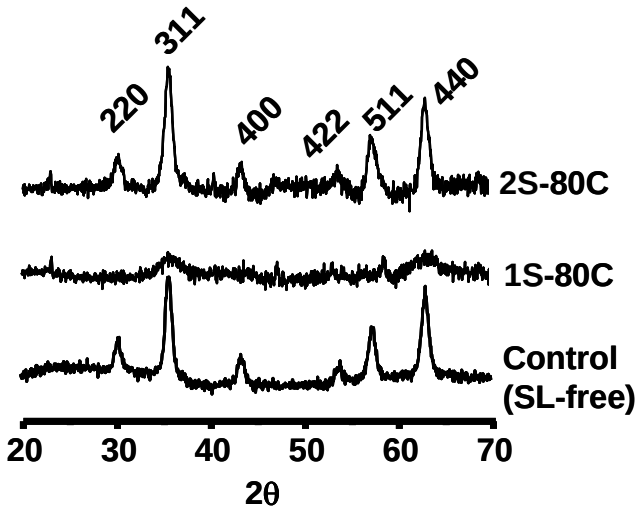

Figure 1 – X-ray diffraction pattern of the sophorolipid-containing iron oxide nanoparticles obtained at 80°C in the two-steps (2S-80C) and one-step (1S-80C) synthesis processes. For sake of comparison, a control, sophorolipid-free, diffraction pattern of iron oxide nanoparticles is also shown. Reported values relate to the Miller (hkl) indices of the Bragg diffraction planes.

TEM images and the corresponding particle size distributions are presented in Figure 2. All samples are composed of spherical nanoparticles whose size and homogeneity depend on the synthesis conditions. The two-steps synthesis, 2S-80C and 2S-RT, provides particles whose average diameter is, respectively, 8.5 nm and 4.5 nm. As reported previously, the higher the synthesis temperature, the larger the average particle size.[21] In both cases, the particle size distribution is comparable (± 2 nm) even if at room temperature bare particles as large as 12 nm can be observed. When SL is used since the beginning of the reaction, the particle size distribution of the final material is consistently different according to the temperature employed: at room temperature (Figure 2, sample 1S-RT), it is broader, going from 3 to more than 20 nm while at T= 80°C the sample 1S-80C is composed of very small nanoparticles, with an average diameter of 2.8 ± 1 nm, if one disregards spurious aggregation on the TEM grid most likely due to the drying process.

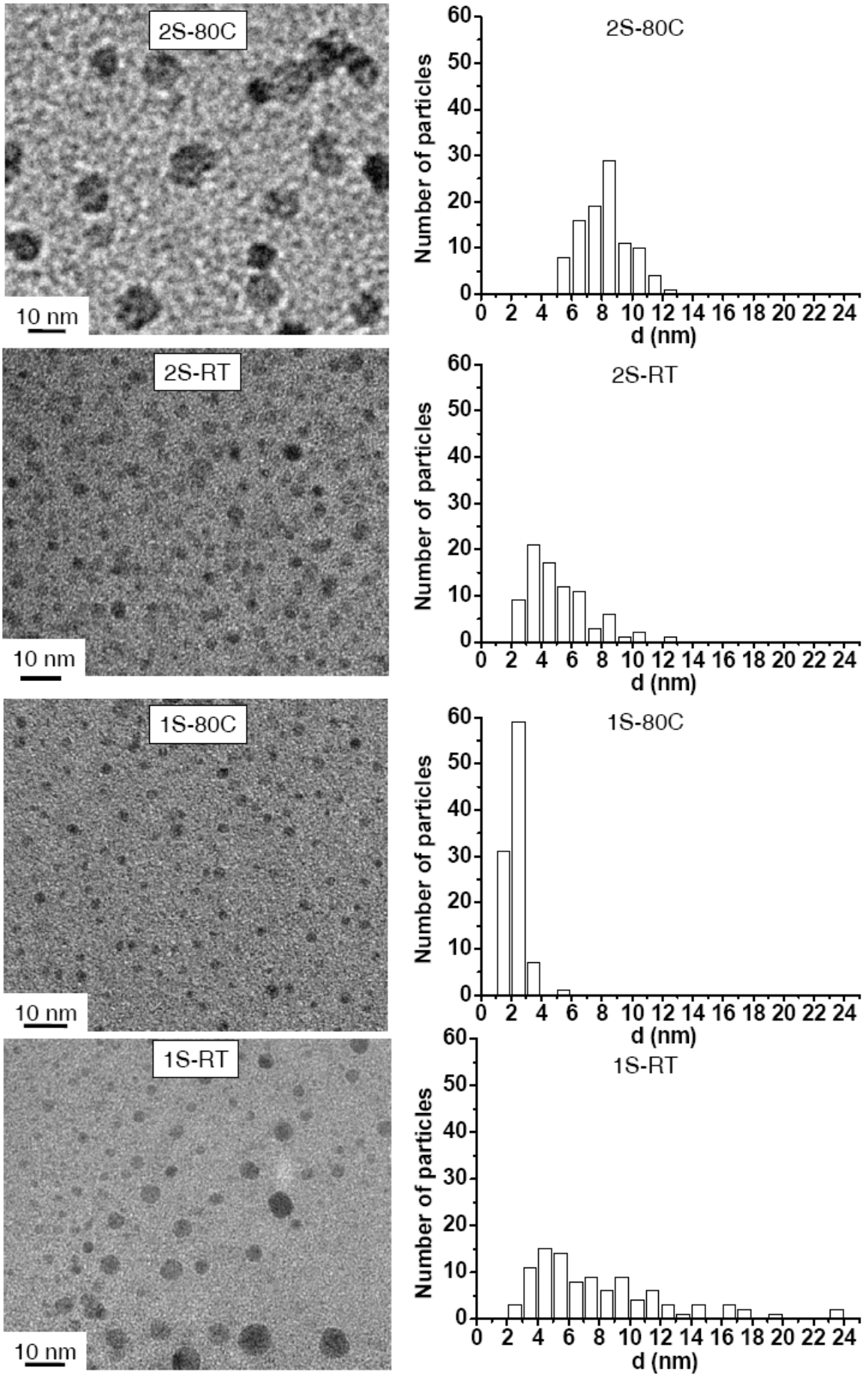
2S-80C
10 nm
2S-80C
Number of particles
d (nm)
2S-RT
10 nm
2S-RT
Number of particles
d (nm)
1S-80C
10 nm
1S-80C
Number of particles
d (nm)
1S-RT
10 nm
1S-RT
Number of particles
d (nm)

Figure 2 – TEM and particle size distribution (PSD) of one-step (1S) and two-steps (2S), sophorolipid-containing, iron oxide nanoparticles at room temperature (RT) and at T= 80°C (80C). PSD have been directly obtained from TEM images after manual counting on at least 100 particles.|

As initially observed by XRD and Mössbauer spectroscopy, and finally confirmed by TEM experiments, one-step and two-steps procedures provide sensibly different materials. Additional confirmation on the nature of the metal oxide particles in the different samples could be obtained by SEM/EDAX experiments, which allowed the quantitative analysis of the elemental Fe/O ratio (Table 1). Interestingly, all one-step syntheses show a rather low Fe/O ratio (< 0.45) with respect to the two-steps material (0.69 for 2S-80C). A comparison with the theoretical values provided in the same table confirms that the chemical composition of the one-step samples is very close to the theoretical Fe/O value expected for ferrihydrite. On the other hand, the value found for the two step samples agrees well with the dominant presence of γ-Fe_2O_3.

Table 1 – Experimental Fe/O ratio values obtained by SEM/EDAX for few selected materials obtained in the one-step and two-steps synthesis. Theoretical Fe/O values for ferrihydrite and γ-Fe_2O_3 are also provided.

1S-RT	1S-80C	2S-80C	Ferrihydrite $Fe_5HO_8 \cdot (4H_2O)$[20]	γ-Fe_2O_3
0.43 ± 0.02	0.36 ± 0.13	0.69 ± 0.07	0.41	0.67

To better understand the structural differences between one-step and two-steps synthesis, one should look at the formation of poorly ordered iron oxides. This was shown for example on supersaturated Fe^{3+} solutions,[22] but also when complexing ligands are used, as they modify the hydrolysis rate of the cation, as shown for acetate and EDTA on Fe(III).[23] Sophorolipids contain a carboxylic acid group, which is notorious for its affinity towards ferric and ferrous ions. Given the lack of literature studies on the specific interaction between sophorolipids and iron in water, we have looked at the published results on the co-reaction between iron salts and common organic acids. For instance, citric acid has a strong influence on the oxidation kinetics of Fe(II) under oxygen, and which is reduced at specific amounts of COOH groups in solution (citrate/Fe(II) > 0.01).[24] If goethite is generally obtained, lepidocrocite formation is promoted upon addition of citric acid. Interestingly, above citrate/Fe(II) > 0.01, non-crystalline oxides are actually formed. Authors attributed these effects to the retarded formation and hydrolysis of iron(III) species, which were also complexed by citrate thus modifying the crystallization process. Retarded hydrolysis of Fe(III) in presence of citrate

ions was also reported by Kandori.[25] In this work, addition of as low as 0.5 mol% of citrate to a ferric chloride solution reduced the size of the formed α- and β-FeOOH material. Above 1 mol%, amorphous particles were formed. In addition, Bee et al.[26] have shown that use of citrate ions have a large influence on the size of maghemite nanoparticles obtained from a Fe(II)/Fe(III)= 0.5 mixture: above 2.5 mol% of citrate, nanoparticles below 2.5 nanometers are obtained. In our synthesis procedure, the molar amounts of COOH and iron salts are comparable, indicating that the presence of small nanoparticles is compatible with the employed synthesis conditions, if compared to references 25 and 26. Since in these works authors use citrate ions (three carboxylate groups), the normalized COOH/(Fe(II) + Fe(III)) molar ratio used in those studies should be multiplied by a factor three. Even under these conditions, the amounts of available COOH used in this work is much higher, meaning that unexpected results in terms of iron oxide structure can be obtained. The first point concerns the fate of Fe(II), which is not found in none of the final oxides. Even if we tried to limit the presence of oxygen, oxidation of Fe(II) has probably occurred during the reaction. Then, as discussed in Ref. 25, complexation of Fe(III) by the COOH group of sophorolipids has undoubtedly modified its hydrolysis-condensation kinetics directing towards the formation of the poorly ordered two-line ferrihydrite, where complexation of Fe(II) prior to oxidation should probably not be neglected.[24] Either control of the hydrolysis/condensation kinetics of iron salts in presence of sophorolipids (for example, by adjusting the SL/iron molar ratio) or setting a post-synthesis treatment, as reviewed by Blesa,[27] are undoubtedly necessary to tune the final iron oxide structure. Nevertheless, these aspect are out of the scope of this work.

Functionalization

FT-IR response of SL allows a better description of the nanoparticle functionalization. The FT-IR spectrum of pure acidic SL is shown in Figure 3 and it displays, among others, the following important resonances: =CH stretch (ν= 3004 cm^{-1}), SL aliphatic backbone (ν= 2920, 2850 cm^{-1}), C=O group in COOH (ν= 1705 cm^{-1}), C=O group in COO^- (ν= 1535, 1418 cm^{-1}), COH and CO in sophorose (ν= 1069, 1024 cm^{-1}). After synthesis, the sophorolipid shows the following features in the SL-functionalized iron oxide nanoparticles system:

- The presence of the symmetric and antisymmetric stretching bands of the aliphatic backbone (ν= 2920, 2850 cm^{-1}) shows that SL are still largely present on the nanoparticle surface, even after multiple washing steps. In addition, the absence of any X-ray diffraction pattern that can

be attributed to SL (Figure 1) indicates that they do not crystallize at the nanoparticle surface after drying.

- The 3004 cm^{-1} resonance is detected. Even if of very low intensity, this peak is generally attributed to the =CH vibration of the oleic acid moiety. Its disappearance indicates that complexation on the nanoparticles can occur through the C=C double bond.[28] It was shown before that the C=C double bond is engaged in the complexation of SL-functionalized silver[15a] and cobalt[15b] nanoparticles. In the case of iron oxide nanoparticles, this mechanism does not seem to be the case for the samples prepared at room temperature while that may occur for the high-temperature derived samples, where this resonance is difficult to see.

- The COOH functional group (ν= 1705 cm^{-1}) is largely reduced in intensity while two resonances, ν= 1535, 1418 cm^{-1}, mark the presence of COO^- (asymmetric stretching - ν_{as} - and symmetric stretching - ν_s - vibrations, respectively). This behaviour is attributed to the complexation of the iron oxide surface by the carboxylate group of the sophorolipid and is in agreement with the synthesis conditions. It was established before that the difference, $\Delta = (\nu_{as} - \nu_s)$, can be related to the way carboxylates bind to the metal oxide surface. For $\Delta > 200$ cm^{-1}, a monodentate binding occurs; for $\Delta < 110$ cm^{-1}, a bidentate binding takes place while for $140 < \Delta < 200$ cm^{-1}, a bridging mechanism best describes the carboxylate-metal coordination. One should nonetheless observe that data obtained from such a simple calculation are qualitative because of the presence of the CH bending at about 1436 cm^{-1}, which may overlap with COO^- stretching resonance, hence inducing an erroneous attribution of this peak. In our materials, we find that $\Delta \sim 130$ cm^{-1} for both one-step derived samples, suggesting a possible bridging coordination mode, while it decreases to $\Delta \sim 115$ cm^{-1} for both two-steps derived samples, indicating a possible bidentate binding instead,[29] even if coexistence of both mechanisms should not be excluded.

- The COH groups of the sophorose head, whose resonances are detected in the region between 1160 and 750 cm^{-1}, might also be involved in the complexation of the iron oxide surface, as already described for similar systems.[30] The 1070 and 1020 cm^{-1} bands, attributed to a C-O stretching coupled with C-C stretching and O-H deformation, do not display any significant shift throughout all samples-set. This is also the case for the resonance at 1160 cm^{-1} (C-O-C glucosidic linkage stretch coupled with C-OH stretch and OH deformation). Even if these data indicate that, for most samples, sophorose is probably not involved into hydrogen bonding with the iron oxide surface, a competing complexation mechanisms of iron by COH groups should not be excluded, as largely discussed by Weissenborn et al.[30] The region below

1000 cm^{-1}, where carbohydrate ring vibration (ν= 935, 710 cm^{-1}), breathing modes (ν= 765 cm^{-1}) and C_1H deformation (where C_1 is the anomeric carbon of sophorose) appear (equatorial C_1H deformation: ν= 850 cm^{-1}; axial C_1H deformation: ν= 890 cm^{-1}) are typically looked at to put in evidence any eventual complexation mechanism. The band at ν= 890 cm^{-1}, which appears in both pure and adsorbed SL, is related to the axial C_1H deformation of the β-D-glucose units.[31] In case of conformational changes, which were described for carbohydrate-complexed iron oxide systems,[30] this band is expected to shift by at least 40 cm^{-1}, which is not the case here for none of the samples, suggesting that complexation of surface iron by sophorose does not occur. Nonetheless, even if we must also point out the appearance of a new band at about ν= 820 cm^{-1}, though of different intensity, in both two-steps samples, and a peak at 770 cm^{-1} in the 1S-80C sample, we are unable to draw any conclusion due to the lack of their clear attribution. In particular, the glucopyranose ring breathing vibration of adsorbed sophorose could be related to the peak at 770 cm^{-1}, as suggested for the adsorption of different polysaccharides on hematite,[30] but unfortunately its absence in the pure SL spectrum does not allow us proper comparisons.

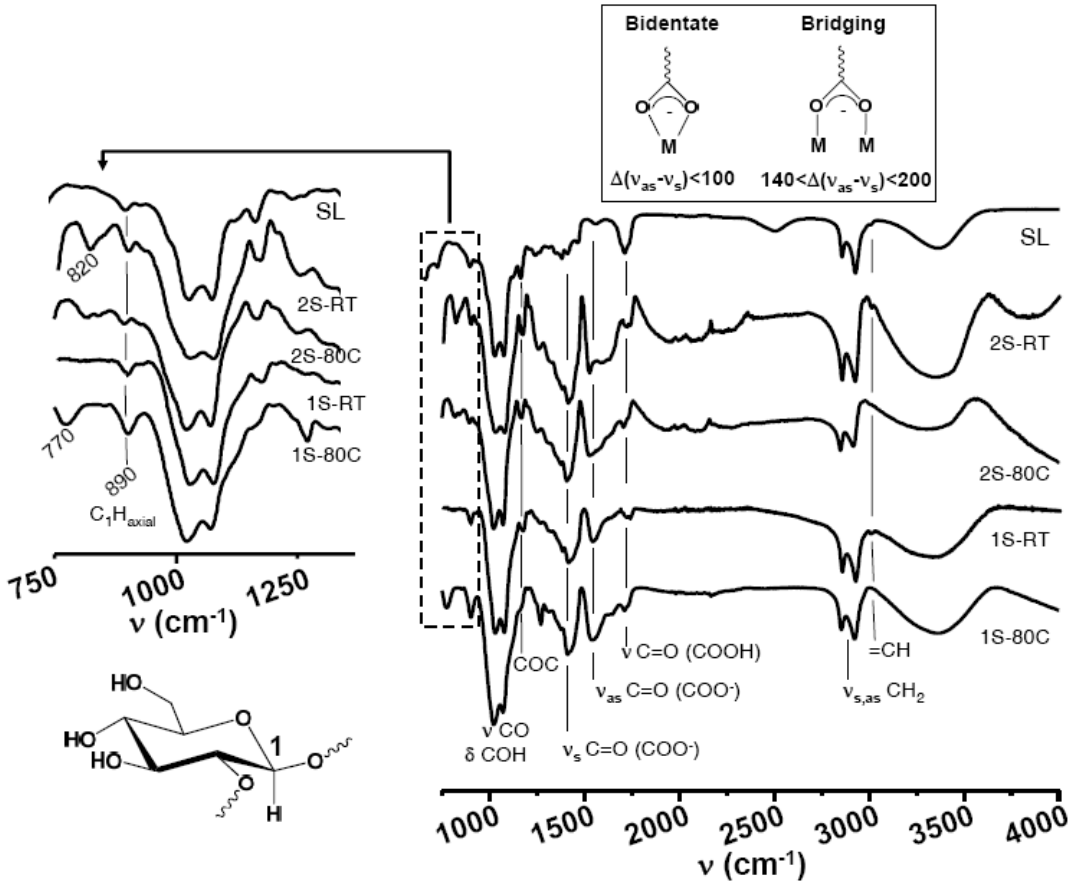

Figure 3 – FT-IR spectra of pure sophorolipid (SL) and SL-functionalized iron oxide nanoparticles obtained at room temperature (RT) and at T= 80°C (80C) in the one-step (1S) and two-steps (2S) synthesis process. On the left, the 750 – 1250 cm^{-1} region is highlighted. The anomeric axial C_1H on the β-D-glucose (left) and the bidentate/bridging coordination modes (top, indicated values are given in cm^{-1}) are represented for sake of clarity. $\Delta(\nu_s-\nu_{as})$ refers to the difference between the symmetric and anti-symmetric stretching vibrations of the COO^- group in the 1400-1550 cm^{-1} region.

According to the FT-IR analysis, it seems clear that iron oxide nanoparticles are functionalized by SL mainly via the carboxylate group and, in the T= 80°C samples, possibly by the C=C double bond of the oleic acid moiety, which it may be expected to provide better stability. Nevertheless, several questions concerning their stability in water and salt-containing medium and the accessibility of sophorose are still open. Previous works on this topic[15] briefly discussed the stabilization of SL-coated Ag and Co nanoparticles in water using FT-IR arguments but no specific experiments showing the stability of SL-coated particles and accessibility of sophorose were given. In the next section, we try to better illustrate this point.

Colloidal stability

The colloidal stability in water of the freshly synthesized SL-derived nanoparticles solutions strongly varies with the synthesis conditions. First of all, if no SL are employed at all, a black, water-demixed, precipitate is always obtained and no stable dispersion is achieved. Even if this is a well-known result, a rapid demonstration, which will be exploited further as a term of comparison, can be obtained through UV-Vis spectroscopy, which is qualitatively used here to evaluate the effect of filtering on non-functionalized nanoparticles in water and, consequently, their aggregation. Figure S2 in Supplementary Information shows the UV-Vis spectra of a blank solution of non-functionalized iron oxide nanoparticles, which have been dispersed in water through sonication (0-labelled spectrum) and after filtration (1-labelled spectrum). Clearly, one single filtration step (ϕ= 0.20 μm) is enough to completely reduce the UV-Vis signal of the blank sample; the lack of any exploitable signal in the complementary DLS experiment recorded on the filtered sample confirms that all nanoparticles have been efficiently removed from the solution.

The results are completely different when SL are employed instead. In the two-steps synthesis, 2S-80C and 2S-RT samples correspond to a stable colloidal solution of maghemite nanoparticles in coexistence with a black/brown precipitate, which is probably due to nanoparticle aggregation before SL-addition and/or insufficient complexation by SL. At 80°C, the solution is clearly darker than in the experiment performed at room temperature, suggesting that either SL functionalization is more efficient, even if FT-IR experiments do not provide a clear-cut proof, or aggregation phenomena among nanoparticles before SL surface coating are reduced. Similar results are obtained on one-step experiments at room temperature while at T= 80°C, a homogeneous, monophasic, brownish stable colloidal solution is obtained instead, as also in Ref. 26 for citrate-derived iron oxide nanoparticles. All SL-derived colloidal solutions are stable over more than a year and centrifugation is not enough to fully recover the nanoparticles for the synthesis at T= 80°C, for which an excess of ethanol is required to precipitate the material. This qualitative observation indicates the strong sophorolipid complexation effect and the steric hindrance of the sophorose group preventing particle aggregation in solution.

Particle size distribution (PSD) obtained from DLS experiments in Figure 4a provides a good picture on the colloidal stability of SL-complexed nanoparticles in water. The number-weighted PSD shows that all samples are mostly constituted of nanoparticles whose diameter falls below 30 nm, even if intensity-filtered PSD (proportional to the sixth power of the particle radius, not shown here) indicates the existence of larger objects in some samples. For instance, one can find that two-steps samples, and 2S-RT in particular, have average sizes

varying between 60 and 100 nm; on the contrary, that seems to be less the case for samples obtained in one-step synthesis. At the moment, we attribute this to either spurious very large particles, aggregation in solution or multilayer sophorolipid coating (see following discussion).

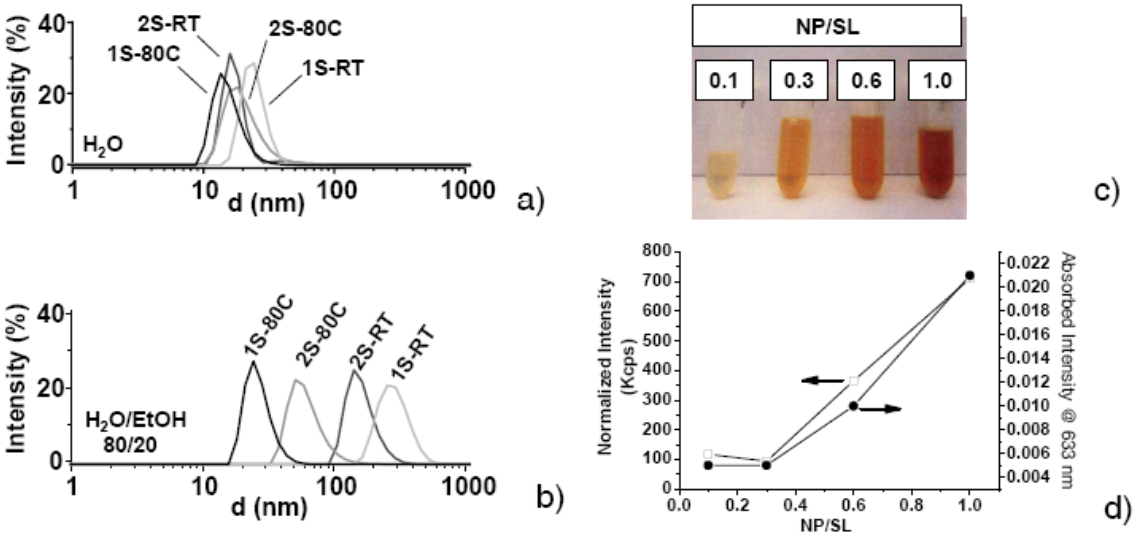

Figure 4 - a) Number-weighted DLS particle size distribution of all SL-functionalized iron oxide samples in water (acronyms and dilution conditions are given in the experimental section); b) Number-weighted DLS particle size distribution of all samples in a 80:20 = H_2O:EtOH (v:v) mixture; c) images showing the concentration effect of a SL-free maghemite nanoparticles redispersed powder in a SL-containing solution at C_{SL}= 50 mg/mL. NP/SL refers to the nanoparticle (NP) over sophorolipid (SL) mass ratio; (d) DLS diffused intensity of solutions presented in (c) in kcps (= kilocounts per second). Values are corrected for the adsorption of the same solution at λ= 633 nm and whose values are presented on the right side of the same figure. A constant shutter value of the DLS apparatus was used for these experiments.

In Table 2, we propose a comparison between the smallest hydrodynamic diameters recorded, d_h (H_2O:EtOH=100:0 column), by DLS with diameters previously measured by TEM, d_{TEM}, that can only be attributed to the size of the oxide particle core alone, because the electron density contrast between SL and the TEM grid support is too low to be measured correctly. According to the synthesis conditions, d_h-values for SL-coated nanoparticles range between 10 and 30 nm, which are all higher than those measured by TEM, as expected. This size range is particularly interesting for biomedical applications, as nanoparticles whose d_h is contained between 10 and 100 nm are optimal for intravenous injections with longer blood circulation times.[3]

Interestingly, one can realize that the difference between d_h and d_{TEM} for all samples, if one excludes 1S-RT, whose broad size distribution in TEM did not allow a precise

measurement, is almost constant: 11.6 ± 3.1 nm. In a previous work we estimated the radius of a spherical SL micelle to be slightly below 3 nm,[12] which, to a first approximation, could correspond to the head-to-tail length of a single SL molecule, L_{SL}. Oi *et al.*[32] have evaluated the thickness of the hydration layer, L_h, of dispersed functionalized metal oxide nanoparticles in water to be between $1.5 < L_h < 2$ nm, by a combination of DLS, static light scattering and small angle neutron scattering (SANS). The average calculated L_h for our samples (1S-RT excluded) is 2.8 ± 1.6 nm,[33] which is consistent with this range of values. Despite the absence of more precise techniques (SANS, for instance), data above suggest the possibility of a monomolecular sophorolipids coating layer for a large part of the nanoparticle population, where the increase of d_h values in DLS experiments could be attributed to the difference in particle core-size. Meanwhile, multilayer sophorolipids coating can also occur and which could actually explain the presence of the larger aggregates detected in the intensity-weighted DLS data discussed above. Looking at Table 2, one realizes that measurements performed on the two-steps (2S) samples show comparable sizes within their error. The comparison of the typical correlograms for samples 2S-80C and 2S-RT (Figure S3 in Supplementary Information) shows a more rapid decay for the curve corresponding to the former sample, which confirms the average smaller size of the scattering particles. For comparison, the faster decaying correlogram of the 1S-80C sample, where particles are the smallest, is also reported in the same figure.

Table 2 – Values of the hydrodynamic diameters, d_h, obtained by the number-weighted DLS experiments for the SL-coated iron oxide nanoparticles in water and in a 80:20 water/ethanol (vol:vol) mixture. d_{TEM} refers to the average diameters measured using TEM (Figure 2). *= size distributions are given in Figure 2.

Sample	d_h (nm) (H_2O/EtOH=100/0)	d_h (nm) (H_2O/EtOH=80:20)	d_{TEM} (nm)*
1S-RT	22.9 ± 4.4	270.1 ± 20.0	3-20
1S-80C	13.7 ± 0.6	24.2 ± 0.1	2.8
2S-RT	19.5 ± 4.5	145.0 ± 6.0	4.5
2S-80C	17.4 ± 2.7	52.8 ± 8.1	8.5

TGA can be used to show the existence of an organic/inorganic material and estimate the area per functional group, as it was shown for, among others, oleic acid-capped maghemite nanoparticles,[34,35,36,37] a system which is closely related to ours. In the Supplementary Information section we describe a simple core-shell model to calculate the available surface

for a given molecule, where the core and the shell are constituted, respectively, of the nanoparticle and its organic coating, whose mass density is supposed to be the same as in its bulk form and constant. It is then possible to calculate (Eq.1 in Supplementary Information) the available surface area per molecule as a function of the core particle radius (R_{in}). This model is rather crude and its accuracy quite weak, first of all because it makes strong assumptions on the density of the organic coating layer and secondly because the exact area per molecule, even in the case of monolayer adsorption on flat surfaces, is dependent on a number of physico-chemical parameters (surface chemistry, pressure, solvent, pH, salt concentration, molecular configuration, etc…). For instance, adsorption of oleic acid, whose molecular structure is close to sophorolipids exception made for the bulkier sophorose headgroup, on flat surfaces is known to provide an area per molecule which varies between 0.1 nm^2 and 0.8 nm^2,[38,39,40] where the latter value is obtained for an horizontal oleic acid configuration.[40] This last parameter is actually particularly important for sophorolipids, for which two forms are known, the lactonic one, where the oleic acid moiety is bent towards the sophorose group, and acidic one, where the oleic acid moiety is free. Few data exist at the moment on the exact description of sophorolipids' molecular conformation in bulk and at liquid/gas interfaces[14,41,42] but it seems highly possible that bending can also occur in the acidic form.[14,42] To this respect, the model used here is reductive as it does not consider neither the effective molecular conformation nor the effective surface density; nevertheless, considering the lack of data on our system if compared to oleic acid, our approach has the merit of allowing quick comparison between similar systems (oleic acid vs. sophorolipids) in which the surface available area per molecule is estimated by TGA and put them in relationship according to the same assumptions, given hereafter.

The idea is to make the hypothesis that for very small nanoparticles, when their radius becomes comparable with the adsorbant typical size, one can reasonably expect important curvature effects on the effective area per molecule. Calculations for a typical oleic acid/nanoparticle system as a function of the particle radius are shown in Figure 5 (straight line). As expected, the available area per molecule decreases for radii below approximately 10 nm. The comparison with real systems is given on the same figure (squares), where the surface area per molecule, calculated according to Eq.2 in Supplementary Information on the basis of published TGA and TEM data, is also provided. Many literature works report 0.20 ± 0.03 nm^2 per oleic acid (about 5 molecules per nm^2) as being a common value[34,36] for nanoparticle radii (R_{in}) below 20 nm. According to the core-shell model employed, below this value one expects the molecular packing to increase, which is not the case. The comparison

between measured and calculated values of area per molecule for oleic acid shows the limits of this model for very small radii but it also reveals to be in fair agreement for very large ones (about 0.22 nm^2 per molecule). The model failure at low radii has also the merit to better visualize the discrepancies existing between different studies. For instance, in Ref.36, authors obtain 0.4 nm^2 per molecule for R_{in} of about 8.0 nm, whereas 0.20 nm^2 should be obtained, which is a value actually found in Ref. 34.

For sophorolipids-capped iron oxide nanoparticles, the available area per molecule can be estimated using our own data (TGA experiments are given in Figure S4 in Supplementary Information). These values can be compared to the ones calculated with Eq.1 given in Supplementary Information (dotted line on Figure 5). The results show a low-density packing for the 1S-80C sample (Figure 5), for which typical values are between 0.2 and 1 nm^2 per molecule, and high density one for the 2S-80C sample, with typical values below 0.1 nm^2 per molecule. The coarse packing of SL molecules in the 1S-80C is comparable with the theoretical value calculated for very large radii and, in this sense, results for SL are similar to what it is observed in Ref. 36,37 for the oleic-acid based samples. Typical results measured by TGA for the 2S-80C sample show, on the contrary, a smaller area per molecule. If specific data on the packing of sophorolipids on nanoparticles are not known, the results obtained for the 1S-80C systems are consistent with what has been reported for sophorolipids (acidic, lactonic and their mixtures) at the air/liquid interface, and whose values range between 0.7 and 1 nm^2 per molecule.[41] Interestingly, smaller values (about 0.5 nm^2 per molecule) were estimated from surface tension experiments for the ester derivatives of acidic sophorolipids on solid flat surfaces.[43] At the moment, the difference between the two samples is hard to explain and the value measured for the 2S-80C system seem too small. The hypothesis concerning the formation of a sophorolipid multiple layer at the nanoparticle surface, as it was proposed for sophorolipid esters on alumina,[43] and as already discussed in the DLS data section is also possible.

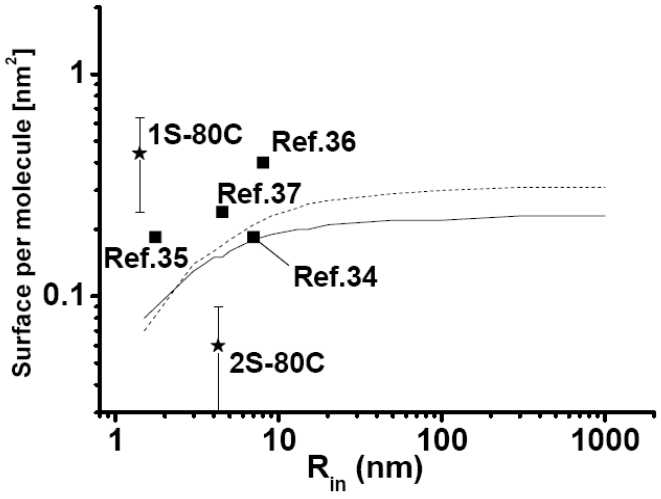

Figure 5 –Lines: calculated exposed surface per molecule as a function of the core nanoparticle radius, R_{in}, according to the core-shell model detailed in the Supplementary Information (Eq.1) for oleic acid (solid line) and sophorolipids (dotted line). Full symbols: data calculated from Eq.2 in Supplementary Information, where $R_{in} \equiv d_{TEM}/2$; m and m_0 have been obtained from TGA analysis. Data for sophorolipids (stars) have been measured in this work while those for oleic acid (squares) have been extracted from references given in the figure.

Colloidal stability in various media.

FT-IR and preliminary DLS experiments strongly suggest that colloidal stability in water is promoted by chemical grafting of sophorolipids on iron oxide nanoparticles and consequent sophorose coating on their outer surface. Here after we confirm these assumptions.

Like all saccharides, sophorose is expected to be less soluble in low-dielectric constant solvents. This is well-known for glucose, for instance, whose solubility in ethanol is very low. At 50 mol% (76 vol%) of ethanol in water, the dielectric constant decreases from 80 to 38[44] and solubility drops from 0.4 g/mL to about 0.1 g/mL if compared to pure water.[45] According to these considerations, we expect nanoparticle aggregation phenomena to occur at a given ethanol/water mixture. The qualitative colloidal stability of the SL-coated iron oxide nanoparticles was first estimated over one week for several H_2O/EtOH mixtures and it was found that the 80/20 (vol:vol) ratio (~ 7 mol% EtOH)[46] was a good compromise in terms of dielectric constant (~ 70)[44] and long term nanoparticle colloidal stability.[47] DLS experiments for the H_2O/EtOH=80/20 (Figure 4b) show an increase of the average hydrodynamic diameter upon addition of ethanol with respect to the pure water solutions (Figure 4a). As summarized in Table 2, upon addition of ethanol to the solution, an increase between 100% and 200% in d_h is observed for samples prepared at 80°C while a ten-fold increase occurs for room temperature samples. We attribute such a large difference between RT and T= 80°C to a

possible SL solubilisation effect of ethanol on more loosely bonded SL molecules at the iron oxide surface, hence inducing nanoparticle aggregations into large aggregates. Since this effect is less pronounced when synthesis temperature is set to 80°C, one could argue a more efficient surface stabilization by sophorose groups.
At the moment FT-IR experiments seem to be give similar results for all samples exception made for the C=C resonance at 3004 cm^{-1}, whose absence in the samples obtained at 80°C may indicate an additional stabilisation of the nanoparticles by the C=C functional group in sophorolipid, hence conferring more stability to these systems.

To confirm the data about the dispersive properties in water of SL-coated iron oxide nanoparticles, we have run a specific experiment where increasing amounts of a dried sophorolipid-free maghemite powder are dispersed in a given volume of SL-containing solution at constant concentration, C_{SL}= 50 mg/mL. DLS experiments were run at constant shutter opening; in this case, the diffused intensity is dependent on the particle concentration. From a visual point of view, the picture shown in Figure 4c illustrates the increasing absorbed intensity of the iron oxide/SL solution as a function of the nanoparticle/SL ratio. As expected, at higher nanoparticle amount (NP/SL= 1), the solution becomes darker. In Figure 4d, the scattered intensity is reported as a function of the NP/SL ratio. These data are corrected by the solution absorption coefficient at λ= 633 nm, as presented on the right axes of Figure 4d. When the amount of nanoparticles increases, the diffused intensity increases as well, directly proving that a higher amount of nanoparticles is dispersed in the solution, thus showing the colloidal stabilizing effect of the SL coating. Similar results are obtained if the order of addition is inversed. By doing this, it is possible to evaluate that for a 1 mg/mL of re-dispersed nanoparticles, one must employ between 0.1 and 0.2 mg of sophorolipids to observe an appreciable increase in the amount of stabilized nanoparticles, detected by DLS (diffused intensity at constant shutter opening, as on Figure 4d). At the same time, the particle size and its distribution become narrower. If no sophorolipids are added, the amount of stable nanoparticles is very low and the size distribution is very large.
To provide further proof of the colloidal stability and show that these systems are interesting candidates for biomedical applications, we run several experiments showing stability towards salt and consecutive filtration steps. These parameters were tested on the SL-functionalized nanoparticles obtained at T= 80°C, when nanoparticles are more stable. Stability towards ionic strength is particularly important because it provides information on the type of ligand-nanoparticle interaction, which, if purely electrostatic, addition of a salt would induce

aggregation; plus, good stability towards salt makes them interesting candidates for biomedical applications. Figure 7 shows the number-weighted DLS and UV-Vis adsorption experiments for the 80°C-synthesized SL-functionalized samples. All samples have undergone 1 filtration step, as indicated on each figure. DLS data show that PSD is essentially unchanged in 0.01 M and 2 M KCl solutions for both 1S-80C and 2S-80C samples (Figure 6a and Figure 6b, respectively) indicating a good colloidal stability upon salt addition at these specific concentrations in water; the main effect is the small increase (5/10 nm) in the measured d_h values. UV-Vis experiments are provided as a complementary tool to indirectly estimate the formation of large (diameter > 0.2 μm) aggregates, which are retained by the filter pores. Upon analysis of the filtered solution, the higher retension in the filter, the stronger attenuation of the UV-Vis signal, as it was shown for the non-functionalized system (Figure S2 in the Supplementary Infomation). Here, UV-Vis spectra recorded on the same samples (Figure 6c,d) indicate that addition of KCl in the 2S-80C system does not affect aggregation much between nanoparticles, at least after one filtration step (comparison with the non-filtered solutions is given later); in fact, the adsorbed intensities for the KCl-free (H_2O), 0.01 M and 2 M solutions are comparable for this sample. On the contrary, the lower signal recorded after KCl addition in the 1S-80C containing solutions indicates that part of this sample has been removed after filtration (rough estimation are reported below). This result suggests that electrostatic interactions between a small fraction of the nanoparticle population induced by salt addition, probably due to either an incomplete or non homogenous surface coverage, are possible.

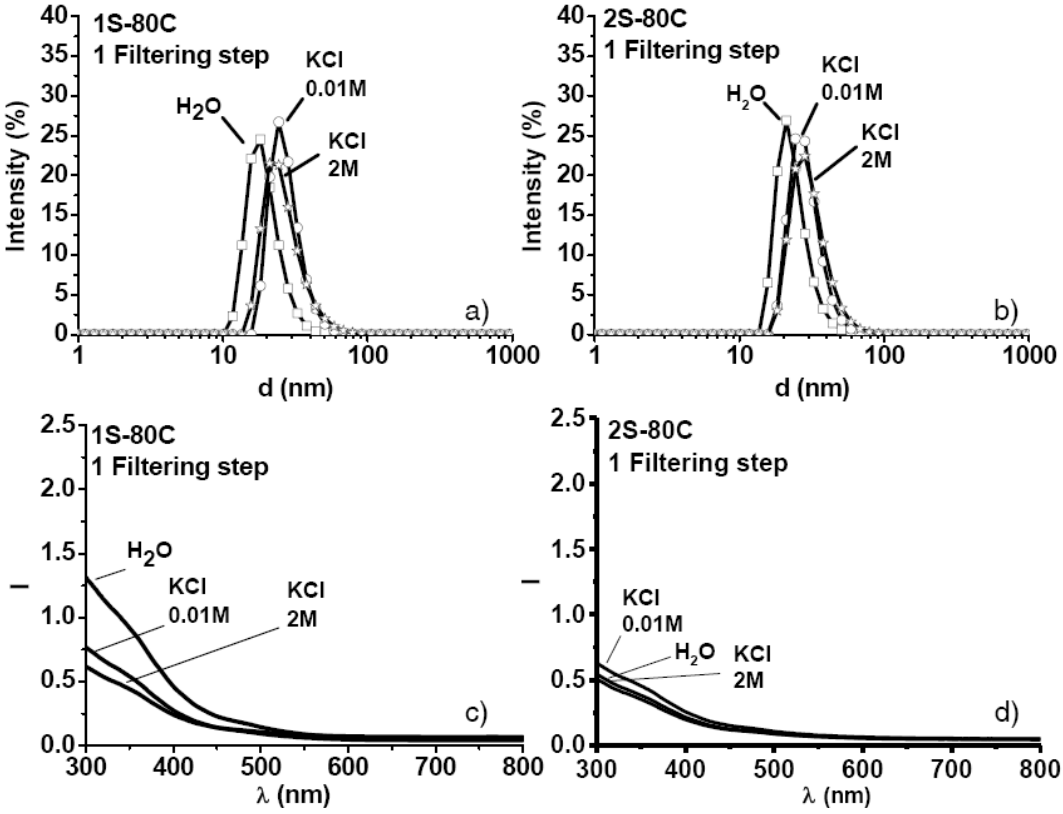

Figure 6 – (a,b) Number-weighted DLS and corresponding (c,d) UV-Vis experiments performed on the single step (1S) and two-steps (2S) synthesis (T= 80°C) systems diluted in H_2O and KCl solutions (0.01 M, 2 M). All samples have been filtered (ϕ= 0.20 μm) once. Dilution conditions are provided in the experimental section. UV-Vis experiments are directly comparable within each system (2S-80C and 1S-80C) because the same batch was used as nanoparticle source.

Filtration is known to have an impact on the ligand stability on the particle surface; for this reason, multidentate binding is generally requested to improve overall stabilization, as nicely shown by Amstad *et al.*[48] We have tested the stability towards this parameter for the 2S-80C and 1S-80C samples in pure water and KCl containing solutions. First of all, one can see that, in large contrast with respect to the blank, non functionalized, Fe_2O_3 solution, one filtration step (1-labelled curves in Figure 8 a,b) for functionalized nanoparticles only contributes to reduce the signals by a factor of 1.4 for 1S-80C and 2 for 2S-80C, whereas all nanoparticles are retained in the filter when functionalization is not performed (Figure S2 in Supplementary Information).

Secondly, DLS (Figure 7 a,b), confirmed by the UV-Vis data (Figure 8 a,b), shows a clear effect of the number of filtration steps on the d_h, which increases from 16 nm to 100 nm on both 1S-80C and 2S-80C samples in pure water. The filtration effect in KCl-containing solutions shows a similar trend. For instance, with increasing KCl amount in the 1S-80C system, one qualitatively observes larger values of d_h, as shown in Figure 7 c,e, where UV-Vis experiments (Figure 8 c,e) indicate that the amount of filtered nanoparticles increases

(decreasing UV-Vis signal). On the contrary, addition of the salt induces a relative stabilization in size of the 2S-80C nanoparticles, as one can observe after DLS experiments (Figure 7 d) even if the amount of nanoparticle keeps decreasing (Figure 8 d). At higher KCl content (2M - Figure 7 f), the stability of the nanoparticles is less pronounced, as shown by the double distribution peaks in the two-times filtered sample, indicating that several populations may exist at the same time.

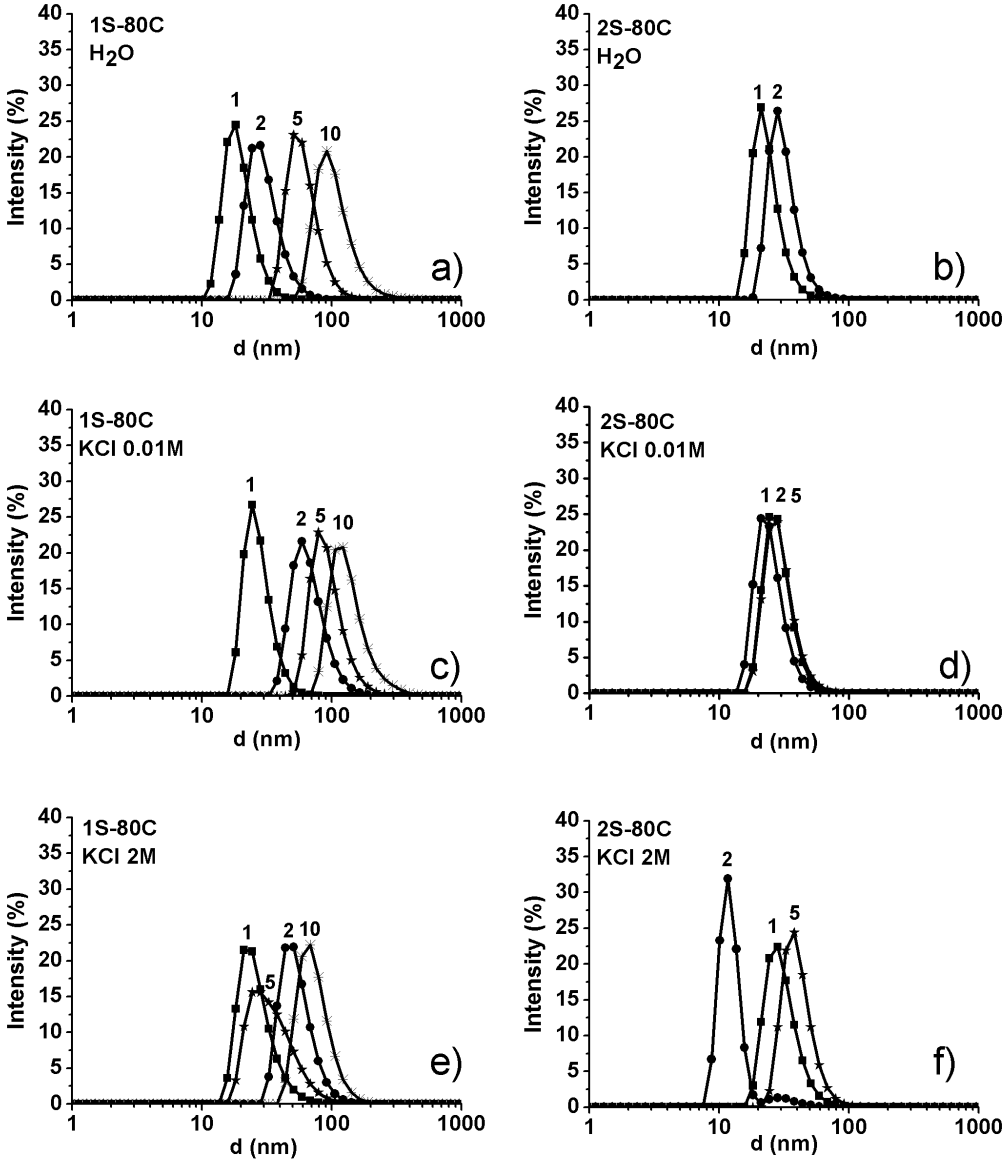

Figure 7 – Number-weighted DLS experiments on 1S-80C and 2S-80C systems in (a,b) H2O, (c,d) KCl at 0.01 M, (e,f) KCl at 2 M. Each number reported on top of the size distribution curves refer to the number of consecutive filtration steps (ϕ= 0.20 μm).

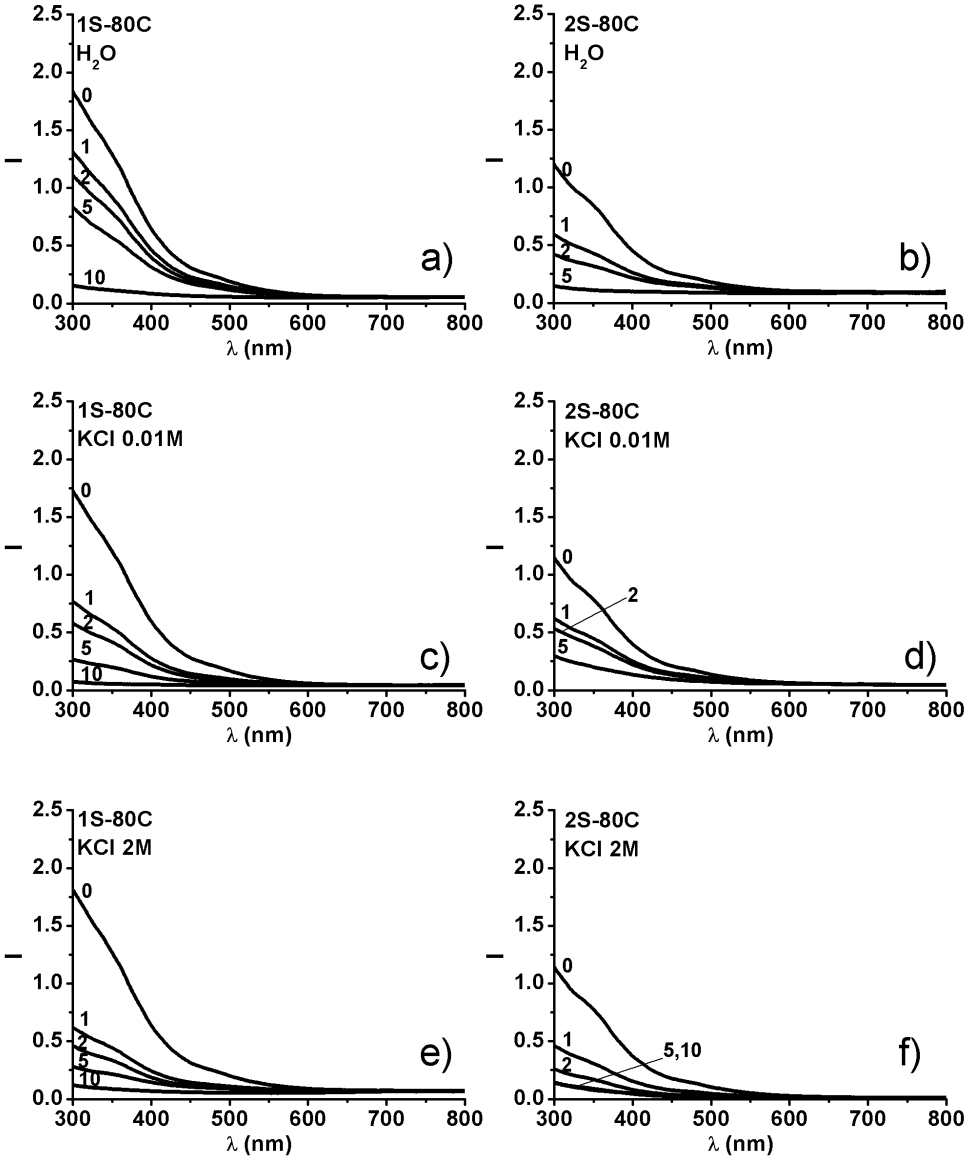

Figure 8 – UV-Vis spectra recorded on 1S-80C and 2S-80C systems in (a,b) H2O, (c,d) KCl at 0.01 M, (e,f) KCl at 2 M. Each number reported next to each spectrum refer to the number of consecutive filtration steps (ϕ= 0.20 μm).

The behaviour of the room temperature-synthesized materials reflects the same trends described above (results not shown). In general, the number of filtration steps (up to 10, at least) induces an aggregation effect of the nanoparticles, whose average measured d_h of the remaining objects never exceeds 100 nm. With respect to Amstad *et al.*,[48] our results seem to be comparable to their intermediate stability range. In particular, the sophorolipids seem to stabilize nanoparticles better than PEG(5)-COOH, PEG(5)-hydroxypyridine and PEG(5)-hydroxydopamine do on a basis of 10 consecutive filtration steps,[48] which, here, induce aggregation up to 100 nm. So far, we could not obtain nanoparticles as stable as those reported in Ref. 48 with PEG(5)-nitroDOPA and PEG(5)-nitrodopamine.

Aggregation upon consecutive filtering is generally attributed to consecutive removal of the stabilizer by the filter itself due to reversible binding on the nanoparticle surface.[49] To improve colloidal stability, reversibility of surface binding is the first point to address. This phenomenon depends on the chemical nature of the functional group but also on the nanoparticle surface charge, solution pH, ionic force, nanoparticle/dispersant ratio, temperature etc… Some of these parameters were tested in Ref. 48. For the sophorolipids/iron oxide nanoparticles studied here, we actually observed that pH and ionic force combined are of paramount importance in terms of colloidal stability. For instance, we qualitatively observed that stability is promoted by low pH, allowing several filtrations. Increase in pH (> 8) promotes binding reversibility with the consequence that most material can be filtered out after one step. On the contrary, stable binding seems to be promoted by a combination of high pH and ionic strength. These phenomena are under current study. The second point to address is the nature of the filter/stabilizer interactions. In fact, one can formulate the hypothesis that different filter materials promote different aggregation behaviour of the nanoparticle according to the specific interactions occurring with the surface stabilizer. For this reason, another way to reduce the aggregation could be the use of well-chosen filter membranes that limit the membrane/stabilizer interactions.

DLS experiments above show that, compared to bare nanoparticles, SL-functionalization stabilizes maghemite and ferrihydrite nanoparticles in both salt-free and salt-containing media (Figure 6), while addition of ethanol induces large variations in size (Figure 4b). According to these data combined with FT-IR, colloidal stability mainly depends on the repulsive steric interactions between the sophorose groups, even if the ligand density at the nanoparticle surface and its conformation are still unclear and may not be equal among all systems, thus playing an important role in the effective stability towards salt addition and filtration. These results are in good agreement with similar systems; for instance, oleic acid-functionalized nanoparticles are known to be highly stable in organic media, the stability being also due to steric repulsion between the fatty acid tails (more theoretical background on the stability of functionalized inorganic particles can be found in Ref.50).[3] As far as the ligand stability is concerned, salt does not seem to contribute to sophorolipids removal, which is probably the case when repeated filtration steps are performed.

Table 3 summarizes the main characteristics of the sophorolipid-functionalized nanoparticles studied in this work. The most stable colloids are obtained at 80°C both after one-step and two-steps, where the latter provides larger nanoparticles. Despite the small discrepancies described previously, both samples are characterized, at least after one filtration step, of

remarkably stable nanoparticles both in water and concentrated KCl solution and whose average sizes for most of the nanoparticle population range between 10 and 30 nm. In comparison, synthesis at room temperature, especially for the two-step synthesis, provides less stable nanoparticles. Finally, use of sophorolipids in the initial batch has a non negligible influence on the iron oxide structure. Iron-complexing phenomena modify the Fe^{2+}/Fe^{3+} stoichiometry and ferrihydrite is obtained instead of maghemite.

Table 3 – Summary of the most relevant structural and colloidal properties of the one-step and two-steps SL-functionalized iron oxide nanoparticles at room temperature (RT) and T= 80°C.

Sample	Synthesis conditions	Structure	d_{TEM} (nm)	d_h (nm)/H_2O	d_h (nm)/KCl 2M	Stability in H_2O	Stability in KCl
1S-RT	- One-step - T= RT	Ferrihydrite	3-20	22.9	27.7	Good	Good
1S-80C	- One-step - T= 80°C	Ferrihydrite	2.8	13.7	21.5	Very good	Very good
2S-RT	- Two-steps - T= RT	Maghemite	4.5	19.5	50.1	Average	Average
2S-80C	- Two-steps - T= 80°C	Maghemite	8.5	17.4	22.1	Very good	Very good

Conclusion

The use of biosurfactants in non-deterging, material science related, applications is a recent research field that takes into account the astonishing and multivalent, yet unknown, properties of some of these compounds. In this work, we have used the acidic form of sophorolipids to functionalize magnetic iron oxide nanoparticles Sophorolipids were added in either one- or two-steps procedure in the typical "Massart" synthesis of iron oxide nanoparticles. In particular, the one-step synthesis provides poorly crystalline ferrihydrite nanoparticles instead of the expected magnetite (or maghemite) structure, indicating a complexation effect of the COOH group on iron metal centers during synthesis. The two-steps approach provides classical γ-Fe_2O_3 nanoparticles. Whatever the protocol, FT-IR experiments show that sophorolipids always interact with the iron oxide surface via their carboxylic group, imprinting a large colloidal stability to the final material. No interactions between sophorose and iron were, on the contrary, observed. According to DLS data combined with UV-Vis experiments, the colloidal stability of sophorolipids-functionalized nanoparticles is good, especially for the materials obtained at 80°C. This has been shown both in pure water and in 0.01 M and 2 M KCl solutions. Further proof of the good complexing ability of sophorolipids is given by specific DLS experiments in which the amount of dispersed nanoparticles in

solution increases with increasing the nanoparticle/sophorolipids mass ratio. The hydrodynamic diameter for a large portion of the nanoparticles varies between 10 and 30 nm in water and it does not become larger than 30 nm for KCl concentrations as high as 2M. Additional experiments in which the colloidal stability was tested towards the number of filtration steps show some aggregation effects between 1 and 10 consecutive steps, even if the size for most of the largest aggregates is always below 100 nm, making sophorolipids interesting candidates for further studies on surface capping agents of nanoparticles for biomedical applications.

The accessibility of the sophorose group at the surface of the nanoparticle is also an important issue for biocompatibility issues. In order to show that a sophorose layer coats the nanoparticle, we have shown via DLS that the average hydrodynamic diameter increases for all samples when an ethanol/water mixture is used as dispersing medium, as carbohydrates are insoluble in alcoholic media.

Acknowledgements

The research leading to these results has received funding from the European Community's Seventh Framework Programme (FP7/2007-2013) under Grant Agreement n° Biosurfing/289219. The authors thank Dr. Moulay-Tahar Sougrati (Institut Charles Gerhardt, Montpellier) for the preparation of the Mössbauer absorbers and the recording of Mössbauer spectra and Patrick Le Griel (Laboratoire de Chimie de la Matière Condensée de Paris, Paris, France) for kind assistance on TEM experiments. Jerôme Fresnais (Physicochimie des Electrolytes, Colloïdes et Sciences Analytiques, Paris, France) is kindly acknowledged for helpful discussions on DLS experiments and Marie Guerard (Ecole Nationale Supérieure de Chimie Rennes, Rennes, France) for her involvement in some synthesis work.

References

[1] R. Bardhan, S. Lal, A. Joshi, N. J. Halas, *Acc. Chem. Res.*, **2011**, 44, 936-946

[2] a) C. Fang, M. Zhang, *J. Mater. Chem.*, **2009**, 19, 6258-6266; b) J. Xie, G. Liu, H. S. Eden, H. Ai, X. Chen, Acc. Chem. Res., 2011, 44, 883-892; c) F. M. Kievit, M. Zhang, *Acc. Chem. Res.*, **2011**, 44, 853-862

[3] S. Laurent, D. Forge, M. Port, A. Roch, C. Robic, L. Vander Elst, R. N. Muller, *Chem. Rev.*, **2008**, 108, 2064–2110

[4] a) C. Fang, M. Zhang, *J. Mater. Chem.*, **2009**, 19, 6258-6266; b) J. Xie, G. Liu, H. S. Eden, H. Ai, X. Chen, Acc. Chem. Res., 2011, 44, 883-892; c) F. M. Kievit, M. Zhang, *Acc. Chem. Res.*, **2011**, 44, 853-862

[5] F. M. Kievit, M. Zhang, *Acc. Chem. Res.*, **2011**, 44, 853-862

[6] a) K. El-Boubbou, D. C. Zhu, C. Vasileiou, B. Borhan, D. Prosperi, W. Li, X. Huang, *J. Am. Chem. Soc.*, **2010**, 132, 4490–4499; b) A. G. Barrientos, J. M. de la Fuente, T. C. Rojas, A. Fernandez, S. Penades, *Chem. Eur. J.*, **2003**, 9, 1909-1921; c) C. Earhart, N. R. Jana, N. Erathodiyil, J. Y. Ying, *Langmuir*, **2008**, 24, 6215-6219; d) B. K. Gorityala, J. Ma, X. Wang, P. Chen, X.-W. Liu, *Chem. Soc. Rev.*, **2010**, 39, 2925–2934

[7] a) Y. C. Lee, R. T. Lee, *Acc. Chem. Res*., **1995**, 28, 321-327; b) T. Buskas, P. Thompson, G.-J. Boons, *Chem. Commun*., **2009**, 5335–5349; c) H. Lis, N. Sharon, *Chem. Rev*., **1998**, 98, 637-674; d) P. H. Seeberger, D. B. Werz, *Nature*, **2007**, 446, 1046-1051

[8] a) C. Earhart, N. R. Jana, N. Erathodiyil, J. Y. Ying, *Langmuir*, **2008**, 24, 6215-6219; b) F. Santoyo-Gonzalez, F. Hernandez-Mateo, *Chem. Soc. Rev*., **2009**, 38, 3449-3462

[9] D. W. G. Develter, L. M. L. Lauryssen, *Eur. J. Lipid Sci. Technol*., **2010**, 112, 628–638

[10] a) M. Maingault, Use of sophorolipids and cosmetic and dermatological compositions, WO/1995/034282A; b) I. N. A. Van Bogaert, K. Saerens, C. De Muynck, D. Develter, W. Soetaert, E. J. Vandamme, *Appl. Microbiol. Biotechnol*., **2007**, 76, 23**–**34; c) A. M. Shete, G. Wadhawa, I. M. Banat, B. A. Chopade, *J. Sci. Ind. Res*., **2006**, 65, 91-11

[11] S. L. Fu, S. R. Wallner, W. B. Bowne, M. D. Hagler, M. E. Zenilman, R. Gross, M. H. Bluth, *J. Surg. Res*., **2008**, 148, 77-82

[12] N. Baccile, N. Nassif, L. Malfatti, I. N. A. Van Bogaert, W. Soetaert, G. Pehau-Arnaudetd, F. Babonneau, *Green Chem*., **2010**, 12, 1564–1567

[13] S. Zhou, C. Xu, J. Wang, W. Gao, R. Akhverdiyeva, V. Shah, R. Gross, *Langmuir*, **2004**, 20, 7926-7932

[14] N. Baccile, F. Babonneau, J. Jestin, G. Pehau-Arnaudet, I. Van Bogaert, *ACS Nano*, **2012**, DOI : 10.1021/nn204911k

[15] a) S. Singh, P. Patel, S. Jaiswal, A. A. Prabhune,C. V. Ramana, B. L. V. Prasad, *New J. Chem*., **2009**, 33, 646–652; b) M. Kasture, S. Singh, P. Patel, P. A. Joy, A. A. Prabhune, C. V. Ramana, B. L. V. Prasad, *Langmuir* **2007**, 23, 11409-11412

[16] S. Dhar, E. M. Reddy, A. Prabhune, V. Pokharkar, A. Shiras, B. L. V. Prasad, *Nanoscale*, **2011**, 3, 575–580

[17] S. Lang, A. Brakemeier, R. Heckmann, S. Spockner, U. Rau, *Chim Oggi-Chem Today*, **2000**, 18, 76-79

[18] a) R. Massart, *IEEE Trans. Magn*., **1981**, 17, 1247; b) R. Massart, V. Cabuil, *J. Chim. Phys*., **1987**, 84, 7

[19] G. Grosse, PC-Mos II; 1.0 ed.; Technische Universität München Munich (Germany), 1993.

[20] J. L. Jambor, J. E. Dutrizac, *Chem. Rev*., **1998**, 98, 2549-2585

[21] L. Babes, B. Denizot, G. Tanguy, J. J. Le Jeune, P. Jallet, *J. Colloid Interf. Sci*., **1999**, 212, 474–482

[22] J. H. A. Van des Woude, P. L. de Bruyn, Coll. Surf., 1983, 8, 55-78

[23] N. B. Milić, P. T. Djurdjević, S. R. Niketić, Z. Anorg. Allg. Chem., 1989, 571, 174-180

[24] G. S. R. Krishnamurti, P. M. Huang, *Clays Clay Miner*., **1991**, 39, 28-34

[25] K. Kandori, M. Fukuoka, T. Ishikawa, *J. Mater. Sci*., **1991**, 26, 3313-3319

[26] A. Bee, R. Massart, S. Neveu, *J. Magn. Magn. Mater*., **1995**, 149, 6-9

[27] M. A. Blesa, E. Matijević, Adv. Coll. Interf. Sci., 1989, 29, 173-221

[28] a)Bala, T.; Swami, A.; Prasad, B. L. V.; Sastry, M. *J. Colloid Interface. Sci*., **2005**, 283, 422 ; b) Wang, W.; Efrima, S.; Regev, O. *Langmuir*, **1998**, 14, 602

[29] a) Y. Lu, J. D. Miller, *J. Coll. Interf. Sci*., **2002**, 256, 41–52; b) L. M. Bronstein, X. Huang, J. Retrum, A. Schmucker, M. Pink, B. D. Stein, B. Dragnea, *Chem. Mater*. **2007**, 19, 3624-3632; c) Nakamoto, K. Infrared and Raman Spectra of Inorganic and Coordination Compounds, Part B: Applications in Coordination, organometallic and Bioinorganic Chemistry, 5th ed., Wiley: New York, 1997, p 387

[30] P. K. Weissenborn, L. J. Warren, J. G. Dunn, *Coll. Surf. A*, **1995**, 99, 27

[31] J. Blackwell, P. D. Vasko, J. L. Koenig, *J. Appl. Phys*., 1970, 41, 4375

[32] L. Qi, A. Sehgal, J.-C. Castaing, J.-P. Chapel, J. Fresnais, J.-F. Berret, F. Cousin, *ACS Nano*, **2008**, 2, 879–888

[33] This value is estimated for the number-weighted population and by considering the difference between the hydrodynamic radius ($d_h/2$) in water, the head-to-tail distance of SL (3 nm) and the nanoparticle core radius ($d_{TEM}/2$): L_h [nm]= $d_h/2$ - 3 - $d_{TEM}/2$, where d_h and d_{TEM} values are given in Table 2.

[34] L. Wang, J. Luo, M. M. Maye, Q. Fan, Q. Rendeng, M. H. Engelhard, C. Wang, Y. Linb, C.-J. Zhong, *J. Mater. Chem*., **2005**, 15, 1821–1832

[35] J. Vidal-Vidal, J. Rivasb, M.A. L´opez-Quintela, *Coll. Surf. A: Physicochem. Eng. Aspects*, **2006**, 288, 44–51

[36] W. H. Binder, H. C. Weinstabl, Monatshefte für Chemie, 2007, 138, 315–320

[37] P. Dallas, A. B. Bourlinos, D. Niarchos, D. Petridis, J Mater Sci, 2007, 42, 4996–5002

[38] J R. Kanicky, D. O. Shah1, J. Coll. Interf. Sci., 2002, 256, 201–207

[39] M. Tomoaia-Cotisel, J. Zsakó, A. Mocanu, M. Lupea, E. Chifu, J. Coll. Interf. Sci., 1987, 117, 464-476

[40] P. M Eriksson, K. B. Sandtröm, J. B. Rosenholm, Pharma. Res., 12, 1995, 715-715

[41] M. Chen, C. Dong, J. Penfold, R. K. Thomas, T. J. P. Smyth, A. Perfumo, R. Marchant, I. M. Banat, P. Stevenson, A. Parry, I. Tucker, R. A. Campbell, Langmuir, 2011, 27, 8854-8866

[42] J. Penfold, M. Chen, R. K. Thomas, C. Dong, T. J. P. Smyth, A. Perfumo, R. Marchant, I. M. Banat, P. Stevenson, A. Parry, I. Tucker, I. Grillo, Langmuir, 2011, 27, 8867-8877

[43] L. Zhang, P. Somasundaran, S. K. Singh, A. P. Felse, R. Gross, Colloids and Surfaces A: Physicochem. Eng. Aspects, 2004, 240, 75-82

[44] H. Yilmaz, *Turk. J. Phys*., **2002**, 26, 243-246

[45] L. A. Alves, J. B. Almeida e Silva, M. Giulietti, *J. Chem. Eng. Data*, **2007**, 52, 2166-2170

[46] According to Fig.2 in Y. F. Yano, J Coll. Interf. Sci., 2005, 284, 255-259, at about 7 mol% of ethanol in water, a minimum value of the molar partial volume of ethanol in water is recorded with respect to a surface excess. Nevertheless, for an exposed surface of 1 cm^2 (typical for DLS cuvettes), only $7.0 \cdot 10^{-5}$ moles of ethanol lay on the surface. In our system, that represents only 1.4 % of the total added ethanol. For this reason, it is reasonable to believe that such a demixing behaviour, typical for all alcool/water misture, has practically no influence on our system.

[47] No macroscopic nanoparticle aggregation phenomena were observed for over one month after dilution

[48] E. Amstad, T. Gillich, I. Bilecka, M. Textor, E. Reimhult, *Nano Lett*., **2009**, 9, 4042-4048

[49] E. Amstad, M. Textora, E. Reimhult, Nanoscale, 2011, 3, 2819-2843

[50] B. Vincent, J. Edwards, S. Emment, A. Jones, *Colloids Surf*. **1986**, 18, 261-281